Journal of Materials Chemistry C

PAPER

View Article Online
View Journal | View Issue

Cite this: J. Mater. Chem. C, 2014, 2, 8691

Photophysical properties of ionic liquid-assisted porphyrin nanoaggregate–nickel phthalocyanine conjugates and singlet oxygen generation†

Sadananda Mandal, Simanta Kundu, Santanu Bhattacharyya and Amitava Patra*

Received 15th July 2014
Accepted 16th August 2014

DOI: 10.1039/c4tc01543f

www.rsc.org/MaterialsC

In this report, we demonstrate the formation of ionic liquid (IL)-assisted zinc octaethylporphyrin (ZnOEP) nanoaggregates which is confirmed by field emission scanning electron microscopy (FE-SEM) and atomic force microscopy (AFM) studies. A large red shifted emission of ZnOEP nanoaggregates in comparison to ZnOEP in DCM confirmed the H aggregation which is due to intermolecular porphyrin–porphyrin (such as π–π/hydrophobic) interactions. The steady state and time resolved spectroscopic studies unambiguously confirm the H-aggregation formation of porphyrin molecules during nanoaggregate formation. The significant quenching of the fluorescence spectrum and the shortening of decay time of porphyrin nanoaggregates imply an efficient (89%) energy transfer from porphyrin nanoaggregates to phthalocyanine. Furthermore, the emission band observed at 1270 nm unambiguously confirms the singlet oxygen ($^1O_2$) generation from ZnOEP nanoaggregates which opens up further prospects in designing new IL-assisted porphyrin nanoaggregates for their application in photodynamic therapy.

Introduction

During the last decades, significant attention has been paid to aggregated nano-structures of various organic molecules to find out potential applications in photodynamic cancer therapies, artificial light harvesting, opto-electronic devices and various sensor technologies.[1–8] In particular, porphyrinoid-(free base porphyrins or metalloporphyrins) based nanostructures due to π–π stacking interactions are of great interest for versatile applications in sensing, light harvesting, photocatalytic and organic photovoltaics due to their excellent photophysical, photochemical, and electrochemical properties.[9–11] Hasobe *et al.* have demonstrated that porphyrin-based nano-architectures are suitable for light energy conversion.[12,13] Recently, they have synthesized CTAB-assisted TiO_2 doped zinc *meso*-tetra(4-pyridyl)porphyrin hexagonal nanocylinders which exhibit efficient hydrogen evolution under visible light irradiation.[14] McHale and his co-workers have reported that porphyrin-based self-assembled structures have potential use in light harvesting and solar cell systems.[15] Furthermore, surfactant-assisted nanospheres and nanorods of zinc *meso*-tetra(4-pyridyl) porphyrins have also been reported recently, which are being used for photocatalysis.[16–18] The tuning factors of the porphyrin aggregation in aqueous solution depend on the structure of porphyrin, concentration, pH and counter ions of inorganic salts in the medium.[19] Furthermore, the aggregation behavior of porphyrin in aqueous solution can be controlled by IL. Wu *et al.* have reported the J-aggregation behavior of diprotonated tetrakis(4-sulfonatophenyl)porphyrin in aqueous solution in the presence of the hydrophilic IL 1-butyl-3-methylimidazolium tetrafluoroborate.[20] Zhang *et al.* have investigated the self-assembly and supramolecular chirality of a dianionic tetrakis(4-sulfonatophenyl)porphyrin in the presence of 1-alkyl-3-methyl-imidazolium tetrafluoroborate.[21] In addition, Pandey and his co-workers have reported the J-aggregation of *meso*-tetrakis(4-sulfonatophenyl)porphyrin in an IL solution by varying the amount of acid concentration and poly(ethylene glycol).[22,23] All the preceding examples of IL-assisted porphyrin aggregation clearly demonstrate that IL plays an important role in the porphyrin aggregation. ILs are widely used as solvents, reactants, capping agents or templates in the synthesis of nanostructure materials with improved properties because of their unique range in the liquid state, good dissolving ability, high thermal stability, high ionic conductivity and non-flammability.[24–30] The supramolecular assembled structures of porphyrin molecules are governed by various non-covalent interactions, such as hydrogen bonding, π–π stacking, hydrophobic and electrostatic interactions, and van der Waals forces, *etc.*[31–35] The supramolecular aggregations are mainly J-type (offset-stack or step like arrangement) and H-type (face-to-face

Department of Materials Science, Indian Association for the Cultivation of Science, Kolkata, 700 032, India. E-mail: msap@iacs.res.in; Fax: +91-33-2473-280; Tel: +91-33-2473-4971

† Electronic supplementary information (ESI) available: Tables T1 and T2, UV-vis spectra, zeta potential curves, photoluminescence spectra, and photoluminescence decay curves of different systems. See DOI: 10.1039/c4tc01543f

arrangement) aggregates, which have unique electronic and spectroscopic properties due to their high structural order.[36]

Recently, zirconium/hafnium porphyrin and phthalocyanine complexes are being used for solar cell devices because porphyrins have strong blue absorption for the B band and phthalocyanine has strong absorption in red for the Q band and as a result, the combination of two is an excellent candidate for solar light collection.[37] Photophysical properties of the porphyrin–phthalocyanine conjugated system have been well studied to date in the molecular state.[38–40] It has been already demonstrated that CdSe QDs can be used to sensitize phthalocyanine (Pc4) *via* resonance energy transfer to generate single oxygen for PDT applications.[41] Furthermore, singlet oxygen generation in photosensitizer doped polymers or silica nanostructures and carbon nanotube photosensitizer conjugate systems has been reported in some recent publications.[42–50] To the best of our knowledge, there is no report on singlet oxygen generation from porphyrin nanoaggregates or porphyrin–phthalocyanine nano-composites which could be useful for photodynamic therapy. Thus, an interesting challenge is to design porphyrin nanoaggregate–phthalocyanine conjugates and understand their photophysical properties.

In this work, we describe a system where Ni-phthalocyanine (NiPc) molecules are attached to IL-assisted ZnOEP nanoaggregates. H-type aggregations of porphyrin molecules are observed during nanoaggregate formation in the presence of IL. An efficient energy transfer from porphyrin nanoaggregates to NiPc is successfully demonstrated. Again, singlet oxygen generation from porphyrin nanoaggregates has been investigated by phosphorescence spectra at the near infra red (NIR) region which might open up further prospects in designing new IL assisted porphyrin nanoaggregates for their application in photodynamic therapy.

Materials

Zinc octaethylporphyrin (Aldrich) [ZnOEP], nickel(II) phthalocyanine-tetrasulfonic acid tetrasodium salt (NiPC) [Aldrich], distilled tetrahydrofuran (THF) [MERCK], dichloromethane (DCM) [MERCK], cetyltrimethylammonium bromide (CTAB) [Alfa Aesar], sodium dodecyl sulfate (SDS) [Aldrich], de-ionized water (MERCK), deuterium dioxide (D_2O) [Aldrich], 1-methyl imidazole (Aldrich) and 1-bromohexadecane (SRL) were used as received for our synthesis. Scheme 1 shows the molecular structures of ZnOEP, NiPC and 1-hexadecyl-3-methylimidazolium bromide.

Experimental section and instrumentation

Synthesis of IL

The IL, 1-hexadecyl-3-methylimidazolium bromide ([HDMIm]Br), was prepared by a reported method using microwave irradiation in a mixture of 1-methyl imidazole and 1-bromohexadecane.[29,51] The prepared IL was then purified by recrystallization and dried in a vacuum and characterized by 300 MHz ^{1}H NMR spectroscopy and ESI mass spectroscopy and the data agreed well with the previously reported values.[51,52] Before using the IL, it was dried under high vacuum at 60 °C to evaporate water.

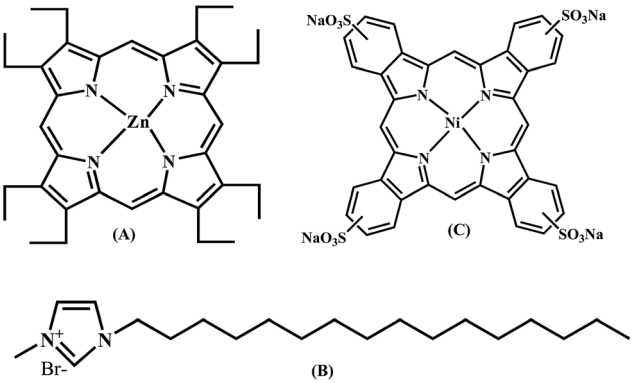

Scheme 1 (A) Zinc octaethylporphyrin, (B) 1-hexadecyl-3-methylimidazolium bromide and (C) nickel(II) phthalocyanine-tetrasulfonic acid tetrasodium salt.

Synthesis of IL-assisted ZnOEP nanoaggregates

The porphyrin nanoaggregate was synthesized by a simple miniemulsion method.[53,54] ZnOEP was properly dissolved in DCM to maintain the 100 μM concentration of ZnOEP. A 500 μL aliquot of this DCM solution was rapidly injected into 2.75 mg of IL containing 10 mL of double distilled water under vigorous stirring for 10–15 minutes followed by ultrasonication for another 15 minutes to form a stable miniemulsion containing small droplets of the ZnOEP solution. The DCM solvent was then evaporated by partial vacuum evaporation for 1 hour at 65 °C. Finally, we obtained a stable aqueous solution of ZnOEP nanoaggregates, which was stable for a week. CTAB- and SDS-assisted ZnOEP nanoaggregates were synthesized following a similar miniemulsion method.[55] The uncapped ZnOEP nanoaggregates were synthesized by the re-precipitation method.[56–58]

Characterization

The morphological characters and sizes of ZnOEP NPs were measured by Field Emission Scanning Electron Microscopy (FE-SEM, JEOL, JSM-6700F) and Atomic Force Microscopy (AFM, VEECO, dicp-II). Room temperature optical absorption spectra were recorded using a UV-vis spectrophotometer (SHIMADZU). Room temperature photoluminescence spectra were recorded using a Fluoromax-P (HORIBA JOBIN YVON) photoluminescence spectrophotometer. For the time correlated single photon counting (TCSPC) measurements, the samples were excited at 375 nm using a pico-second diode laser (IBH Nanoled-07) in an IBH Fluorocube apparatus. The typical full width at half maximum (FWHM) of the system response using a liquid scatter was about 90 ps. The repetition rate was 1 MHz. The fluorescence decays were collected on a Hamamatsu MCP photomultiplier (C487802). The fluorescence decays were analyzed using IBH DAS6 software. The following equation was

used to analyze the experimental time resolved fluorescence decays, $P(t)$;[59]

$$P(t) = b + \sum_{i}^{n} \alpha_i \exp\left(-\frac{t}{\tau_i}\right) \quad (1)$$

Here, n is the number of discrete emissive species, b is the baseline correction ("dc" offset), and α_i and τ_i are pre-exponential factors and excited-state fluorescence lifetimes associated with the i^{th} component, respectively. For multi-exponential decays the average lifetime, $\langle\tau\rangle$, was calculated from the following equation,[60]

$$\langle\tau\rangle = \sum_{i=1}^{n} a_i\tau_i \quad (2)$$

where $a_i = \alpha_i/\sum\alpha_i$ and a_i is the contribution of the decay component. The phosphorescence spectra of singlet oxygen were monitored by using a Fluorolog-3 IHR spectrafluorometer (Jobin-Yvon) equipped with a NIR sensitive photomultiplier (Hamamatsu model: R5509-72) operating at a temperature of 277 K. For the phosphorescence measurement, IL assisted ZnOEP nanoaggregates were synthesized in D_2O media.

Results and discussion

Structural properties and aggregation behavior

Fig. 1 shows the FE-SEM and AFM images of the IL-assisted ZnOEP nanoaggregates. These images unambiguously confirm the formation of spherical porphyrin nanoaggregates by the mini-emulsion method used in this study. The size distribution curve shows that the average diameter of the ZnOEP nanoparticle is about 65 nm and the 3D AFM image shows that the average height of the particles is about 25 nm. The porphyrin nanoaggregate is formed due to the aggregation of porphyrin nanoparticles. A general mechanism of porphyrin nanoparticle formation is as follows: during the ejection of DCM solution of ZnOEP in the micellar solution of IL under stirring conditions, the solution divided into many stable small droplets of the ZnOEP solution by a strong shearing force. The porphyrin molecules are aggregated to form nanoparticles in the hydrophobic micelle when the DCM solvent is evaporated by partial vacuum evaporation.

In general, porphyrins and metalloporphyrins feature two well-defined absorption regions, so-called high-energy B (also known as Soret) and low-energy Q bands. The Soret absorption band corresponds to $S_0 \rightarrow S_2$ electronic transitions, while Q bands correspond to $S_0 \rightarrow S_1$ electronic transitions.[61] Both the B and Q bands arise from π–π^* electronic transitions. Both S_1 and S_2 excitation states are split into the lower- and higher-level energy excited states due to 'H' (face-to-face) or 'J' (edge-to-edge) molecular aggregations.[62] According to the exciton coupling model,[63] the higher excited states are transitionally allowed in the case of H aggregation whereas lower excited states are transitionally allowed for J aggregation. As a result, hypsochromic and bathochromic shifts of absorption spectra occur for H and J aggregations, respectively. In this study, ZnOEP in the DCM solvent shows a very sharp Soret band at 400 nm and Q bands at 530 nm and 567 nm (Fig. 2), indicating a pure monomeric form.[64] However, the hypsochromic shifting of the Soret band (by 11 nm) and bathochromic shifting of Q bands (by 17 nm and 25 nm) are observed for ZnOEP nanoaggregates. A large difference in the spectral shape of the ZnOEP nanoaggregate and ZnOEP monomer is observed. In particular, the calculated FWHM values are 35 nm and 12 nm for the ZnOEP nanoaggregate and ZnOEP monomer, respectively. The observed steady-state spectral changes (blue shift and spectral

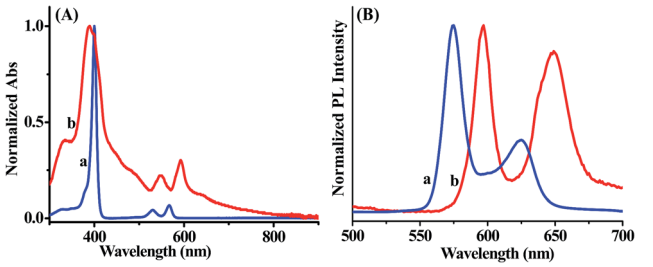

Fig. 2 (A) UV-vis spectra and (B) fluorescence spectra of ZnOEP (a) in DCM solution and (b) in nanoaggregates form.

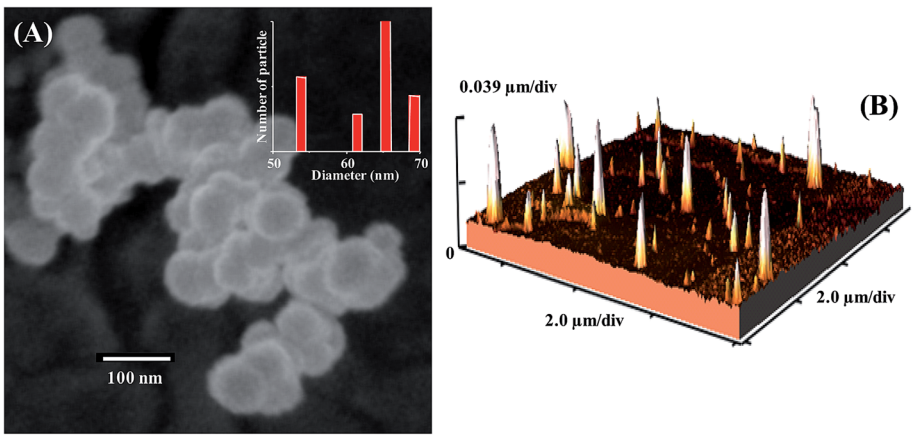

Fig. 1 Images of IL-assisted ZnOEP nanoaggregates (A) FE-SEM and (B) AFM images (3D).

broadening) suggest that the ZnOEP molecules form the H-aggregated state due to the increment of local concentration of ZnOEP inside the IL micelle. One may expect that the spectral shifting is the result of solvatochromism because the monomeric porphyrin molecule and the porphyrin nanoaggregate are in different solvents (the molecular form in DCM and nanoparticles in aqueous solution, respectively). To clarify this point, absorption spectra of ZnOEP are taken in different polar organic solvents in which the porphyrin molecules are soluble and exist as monomers (ESI Fig. S1†). This experiment suggests that ZnOEP has positive solvatochromism properties (*i.e.* bathochromic shift or red shift with increasing solvent polarity). Therefore, the blue shift (with respect to DCM solution) of ZnOEP in the nanoaggregate form (in water, more polar than DCM) unambiguously confirms the H-aggregation of ZnOEP.

Fig. 2B shows the emission spectra of ZnOEP in DCM solution and ZnOEP nanoaggregates. Upon excitation of ZnOEP in the DCM solvent at 375 nm, the fluorescence spectrum exhibits two emission bands at 572 nm (Q^*_{x00}) and 623 nm (Q^*_{x01}), which are the characteristic peaks of ZnOEP chromospheres in the DCM solvent and in good agreement with the previously reported data.[65] In the case of ZnOEP nanoaggregates the emission peaks at 597 nm (Q^*_{x00}) and 647 nm (Q^*_{x01}) are observed. A large red shifted emission (by 25 nm and 24 nm, correspondingly) and lower fluorescence intensity of ZnOEP nanoaggregates in comparison to ZnOEP in DCM are apparently due to the H aggregation (as discussed above) which is induced by intermolecular porphyrin–porphyrin (such as π–π/hydrophobic) interactions and the hydrophobic interaction between porphyrins and long hydrophobic chains of ILs. In this case, the emission spectrum of the H aggregated ZnOEP nanoaggregate is red shifted with respect to that the ZnOEP monomer because the emission occurs from the low energy excited state of H-aggregated species which are transitionally forbidden, and it is further consistent with the previous report of H-aggregates of porphyrin–surfactant complexes by N. Periasamy *et al.*[66]

In order to gain further information on the aggregation behavior of ZnOEP in the nanoaggregate form, the time resolved fluorescence spectra are recorded at the excitation wavelength of 375 nm. Fig. 3 depicts the photoluminescence decay profiles of ZnOEP in DCM and in the nanoaggregate form. In the case of ZnOEP in DCM, at the emission wavelength of 572 nm, the decay curve is fitted mono-exponentially with the life time of 1.48 ns, while at the emission wavelength of 623 nm the decay curve is fitted bi-exponentially with the decay components of 1.48 ns (99%) and 9.80 ns (1%) and the average decay time is 1.56 ns. On the other hand, at the emission wavelength of 597 nm, the decay curve of ZnOEP nanoaggregates is fitted by tri-exponential with the decay component of 0.06 ns (90%), 0.66 ns (8%) and 2.02 ns (2%) and the average decay time is 0.15 ns. At the emission wavelength of 647 nm, the decay curve is also fitted by tri-exponential with the decay component of 0.11 ns (77%), 1.08 ns (18%) and 3.68 ns (5%) and the average decay time is 0.46 ns. All the decay parameters are given in Table 1. After the formation of nanoaggregates, the average decay time of the ZnOEP decreases in both emission bands. The decrease

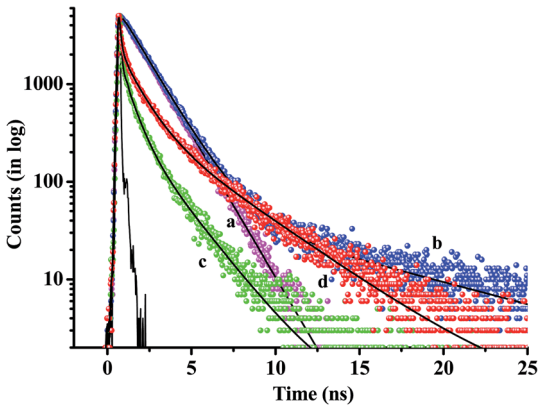

Fig. 3 Photoluminescence decay curves of ZnOEP at the excitation wavelength of 375 nm (a) ZnOEP in DCM (λ_{em} = 572 nm), (b) ZnOEP in DCM (λ_{em} = 623 nm), (c) ZnOEP nanoaggregates in water (λ_{em} = 597 nm) and (d) ZnOEP nanoaggregates in water (λ_{em} = 623 nm).

of decay time of ZnOEP in the nanoaggregate form confirms the H-aggregation of porphyrin molecules.[67]

Photoinduced energy transfer

In the present study, the ZnOEP nanoaggregate–NiPC system has been designed by mixing NiPC molecules with the as synthesized ZnOEP nanoaggregates. The surface of ZnOEP nanoaggregates is positively charged due to the presence of the positive imidazolium group of IL in the outside of the micelle and the NiPC is negatively charged due to the presence of the sulfonate group which is confirmed by the zeta potential study (ESI Fig. S2†). Therefore, NiPCs are attached onto the surface of ZnOEP nanoaggregates by electro-static interaction. Furthermore, the imidazolium group of IL may interact with the NiPC *via* stacking interaction because of their π-planar surface. Recently, Yaku and his co-workers reported that anionic phthalocyanines bind with the G-quadruplex *via* π–π stacking in spite of electrostatic repulsion.[68] To confirm the formation of IL-assisted ZnOEP nanoaggregate–NiPC composite, absorption spectra of NiPC (in the absence and in the presence of IL) have been recorded. When increasing the concentration of IL, the absorption peak at 621 progressively disappears and two strong absorption peaks at 657 nm and 605 nm progressively appear (Fig. 4). This spectral feature indicates the complex formation of NiPC with IL. Since, there is a perfect overlap between the emission spectra of porphyrin and the absorption spectra of NiPC (Fig. 5), thus the photoinduced energy transfer process from porphyrin nanoaggregates to NiPC is highly expected in this composite system. To investigate the energy transfer phenomena, steady state fluorescence and time resolved spectroscopic studies of this composite system have been carried out. Fig. 6 shows the fluorescence emission spectra of IL-assisted ZnOEP nanoaggregates and ZnOEP nanoaggregate–NiPC systems by varying the concentration of NiPC at the excitation wavelength of 375 nm. An enhancement of the quenching efficiency of ZnOEP nanoaggregates in both emission bands is observed with increase in the concentration of NiPC. The values

Table 1 Decay parameters of ZnOEP in the DCM solution and in IL-assisted nanoaggregates at an excitation wavelength of 375 nm

Sample	Emission (nm)	τ_1 (ns) (a_1)	τ_2 (ns) (a_2)	τ_3 (ns) (a_3)	$\langle\tau\rangle$ (ns)
ZnOEP in DCM	572	1.48 (1)	—	—	1.48
	623	1.48 (0.99)	9.81 (0.01)	—	1.56
IL assisted ZnOEP nanoaggregates	597	0.06 (0.90)	0.66 (0.08)	2.02 (0.02)	0.15
	647	0.11 (0.77)	1.08 (0.18)	3.68 (0.05)	0.46

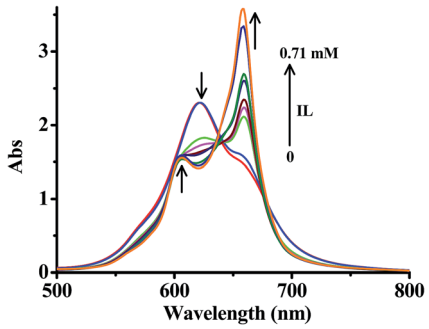

Fig. 4 Absorption spectra of NiPC at different concentrations of IL.

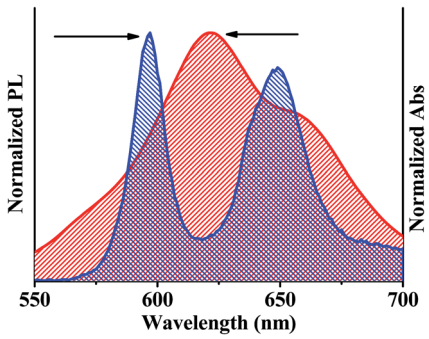

Fig. 5 Overlap spectra between absorption of NiPC and emission of ZnOEP nanoaggregates.

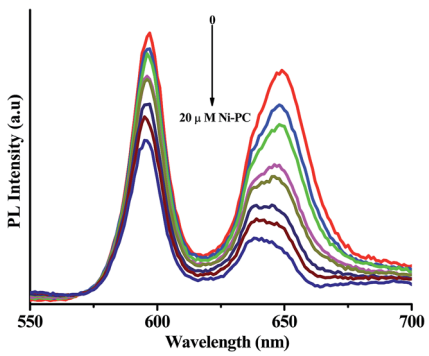

Fig. 6 Photoluminescence spectra of ZnOEP nanoaggregates in the presence of different concentrations of NiPC.

of fluorescence intensity quenching at the emission band of 597 nm are found to be 8, 25 and 38% for 4, 12 and 20 μM concentrations of NiPC, respectively. However, the values of fluorescence intensity quenching at the emission band of 647 nm are found to be 22, 56 and 70% for 4, 12 and 20 μM concentrations of NiPC, respectively. The fluorescence quenching is indicative of the energy transfer from ZnOEP nanoaggregates to NiPC. To understand the energy transfer mechanism, the corresponding fluorescence decay times of ZnOEP nanoaggregates with and without NiPC are measured at both emission bands. Fig. 7 shows the fluorescence decay curves of ZnOEP nanoaggregates with and without NiPC at both

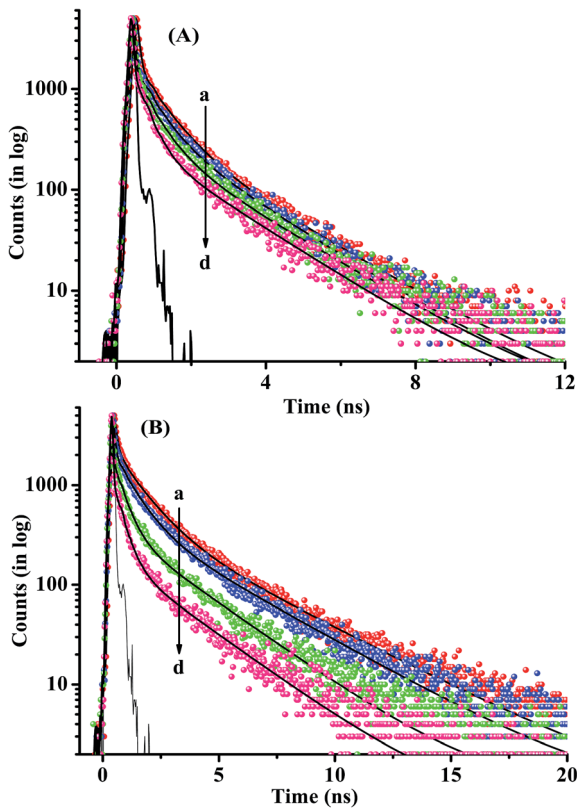

Fig. 7 Photoluminescence decay curves of ZnOEP nanoaggregates at the emission wavelength of (A) 597 nm and (B) 637 nm, in the presence of different concentrations of NiPC (a) 0 μM, (b) 4 μM, (c) 12 μM and (d) 20 μM NiPC (excitation wavelength at 375 nm).

emissions [(A)-597 nm and (B)-647 nm]. All the decay curves are tri-exponentially fitted. At the emission wavelength of 647 nm, the average decay times of ZnOEP nanoaggregates are found to be 0.46 ns, 0.36 ns, 0.13 ns and 0.05 ns for the NiPC concentration of 0, 4, 12 and 20 μM, respectively (Table 2). At the emission wavelength of 597 nm, the average decay times of ZnOEP nanoaggregates are found to be 0.15 ns, 0.10 ns, 0.07 ns and 0.06 ns for the NiPC concentration of 0, 4, 12 and 20 μM, respectively (Table 2). The shortening of decay time of ZnOEP nanoaggregates in the presence of NiPC confirms the energy transfer from porphyrin nanoaggregates to phthalocyanines. For the 20 μM concentration of NiPC, the calculated energy transfer efficiencies are 60% and 89% for the emission wavelength of 597 and 647 nm, respectively. The energy transfer efficiency at 647 nm is higher than that at 597 nm which may be due to the better overlap between the absorption spectra of NiPC and the second emission band of ZnOEP nanoaggregates (overlap integral values are 4.47×10^{-13} and 5.43×10^{-13} M^{-1} cm^3 for the emission wavelength of 597 and 647 nm, respectively).

To understand the importance of aggregated structures of porphyrin and the role of IL in the energy transfer process, we have done some control experiments. Since, IL is also soluble in DCM, hence, the NiPC is transferred to DCM using IL which is being used as a phase transferring agent. Steady state absorption, fluorescence and time resolved spectroscopic data (ESI Fig. S3 and S4†) show no electronic interaction between ZnOEP and NiPC in the DCM solvent. Previously, we have also observed that no energy transfer occurs from the poly (9-vinylcarbazole) (PVK) polymer to ZnOEP in the DCM solvent, whereas, more than 90% energy transfer occurs when ZnOEP is aggregated in PVK nanoparticles.[69] Therefore, aggregation induced nanostructures of ZnOEP are the promising materials involved in the energy transfer process. The UV-vis, photoluminescence and fluorescence decay curves of ZnOEP nanoaggregates (synthesized by the re-precipitation method) with and without NiPC are depicted in the ESI Fig. S5 and S6.† It is found that the fluorescence intensity of ZnOEP nanoaggregates decreases rapidly but the decay time of the ZnOEP nanoaggregates decreases slightly with the increasing NiPC concentration. The calculated energy transfer efficiencies are 54% and 39% for the emission wavelength of 597 nm and 637 nm, respectively. In the case of CTAB (a cationic surfactant)-assisted ZnOEP nanoaggregates, the energy transfer efficiencies are 13% and 18% for the corresponding emission bands. The absorption, fluorescence and fluorescence decay curves of CTAB-assisted ZnOEP nanoaggregates and ZnOEP–NiPC are given in the ESI Fig. S7 and S8.† The ZnOEP nanoaggregates are synthesised in the presence of an anionic surfactant, SDS. We do not observe any significant change in energy transfer from ZnOEP nanoaggregates to NiPC (ESI Fig. S9†). Therefore, the above discussed results imply that IL has played an important role in the energy transfer process from porphyrin nanoaggregates to NiPC. It has been already reported that the stacking interaction occurs between anionic phthalocyanines with the G-quadruplexes.[68] Thus, we believe, the aromatic imidazolium group of the IL facilitates the π–π interaction with anionic NiPC, which enhances the energy transfer efficiency. More investigation is required to understand this phenomenon.

Photosensitization and singlet oxygen generation

Besides the significant energy donating property of the IL-assisted ZnOEP nanoaggregates to energy accepting NiPC molecules (discussed above), they can act as a very good singlet oxygen photosensitizer. The photoinduced singlet oxygen generation has been directly investigated by the phosphorescence spectra at the near infrared (NIR) region. Fig. 8 shows the phosphorescence spectra of singlet oxygen at the excitation wavelength of 375 nm. The emission band observed at 1270 nm, unambiguously confirms the singlet oxygen generation from ZnOEP nanoaggregates. The ZnOEP nanoaggregates generate singlet oxygen by the following ways: during the excitation of ZnOEP nanoaggregates at 375 nm, the nanoaggregates are promoted to the first excited singlet (S_1) state for Q-bands and

Table 2 Decay parameters of IL-assisted ZnOEP nanoaggregates with varying concentrations of NiPC at an excitation wavelength of 375 nm

Sample	Emission (nm)	τ_1 (ns) (a_1)	τ_2 (ns) (a_2)	τ_3 (ns) (a_3)	$\langle\tau\rangle$ (ns)
ZnOEP nanoaggregates	597	0.06 (0.90)	0.66 (0.08)	2.02 (0.02)	0.15
	647	0.11 (0.77)	1.08 (0.18)	3.68 (0.05)	0.46
ZnOEP nanoaggregates + 4 μM NiPC	597	0.04 (0.93)	0.52 (0.05)	1.86 (0.02)	0.10
	647	0.09 (0.81)	0.99 (0.15)	3.55 (0.04)	0.36
ZnOEP nanoaggregates + 12 μM NiPC	597	0.03 (0.94)	0.42 (0.05)	1.79 (0.01)	0.07
	647	0.04 (0.92)	0.55 (0.06)	2.92 (0.02)	0.13
ZnOEP nanoaggregates + 20 μM NiPC	597	0.03 (0.95)	0.43 (0.04)	1.77 (0.01)	0.06
	647	0.02 (0.97)	0.46 (0.02)	2.64 (0.01)	0.05

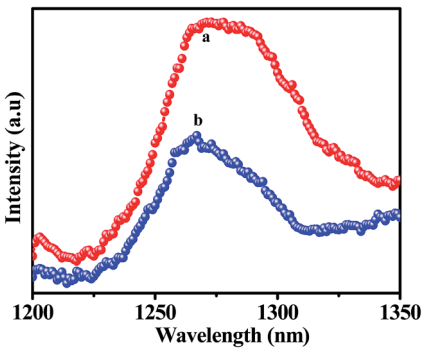

Fig. 8 Phosphorescence spectra of singlet oxygen (a) IL-assisted ZnOEP nanoaggregates (b) IL-assisted ZnOEP nanoaggregates with NiPC at the excitation wavelength of 375 nm.

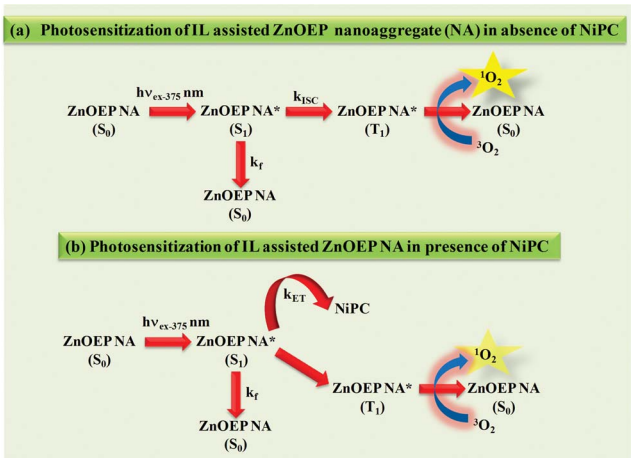

Scheme 2 Schematic representation of pathways of singlet oxygen generation.

the second excited singlet (S_2) state for the B-band. The particle goes down to S_1 from the S_2 state *via* internal conversion. Then, the nanoaggregates undergo intersystem crossing from the S_1 state to the triplet (T_1) state by a nonradiative relaxation process. The triplet state of the nanoparticle eventually transfers energy nonradiatively toward the triplet oxygen and converts to the singlet oxygen (Scheme 2a).[70] However, in the presence of NiPC, the singlet oxygen generation of ZnOEP nanoaggregates is reduced (curve b in Fig. 8). It may be due to energy transfer from ZnOEP nanoaggregates to NiPC which reduces the population of the triplet state of ZnOEP nanoaggregates (Scheme 2b). Therefore, it can be plausibly concluded that ZnOEP nanoaggregates produce an efficient amount of singlet oxygen which may open up further prospects in designing new IL-assisted porphyrin nanoaggregates for their application in photodynamic therapy.

Conclusions

In summary, we have successfully designed IL-assisted ZnOEP nanoaggregates which is confirmed from FE-SEM and AFM analyses. The steady state and time resolved spectroscopic investigation unambiguously confirm the H-aggregated state of porphyrin molecules during nanoaggregate formation. It is seen that no energy transfer takes place from porphyrin to phthalocyanine in an organic solvent while the efficient energy transfer (89%) takes place from IL-assisted ZnOEP nanoaggregates to the NiPC molecules due to close proximity by electrostatic as well as π–π interaction. Furthermore, the IL-assisted ZnOEP nanoaggregates are the better energy donor compared to the uncapped ZnOEP nanoaggregates and surfactant-assisted ZnOEP nanoaggregates due to π–π interaction between IL and NiPC. This remarkably high efficiency of energy transfer in the IL-assisted ZnOEP nanoaggregate–NiPC system opens up further prospects in potential applications as various photo-driven devices. Since, the porphyrin nanoaggregates and the conjugate system can produce an efficient amount of singlet oxygen, these systems may be useful for bio-imaging and therapeutic applications.

Acknowledgements

SERB-DST and "DAE-SRC Outstanding Investigator Award" are gratefully acknowledged for financial support. SM and SK thank CSIR and SB thanks IACS for awarding fellowship. Subrata Das is acknowledged for the technical assistance. Mr Abhishek Bhattacharya (Department of Biochemistry, University of Calcutta) is acknowledged for measuring the phosphorescence spectra.

References

1 J.-M. Lehn, *Science*, 2002, **295**, 2400–2403.
2 Q. Ding, Y.-E. Miao and T. Liu, *ACS Appl. Mater. Interfaces*, 2013, **5**, 5617–5622.
3 B. Khlebtsov, E. Panfilova, V. Khanadeev, O. Bibikova, G. Terentyuk, A. Ivanov, V. Rumyantseva, I. Shilov, A. Ryabova, V. Loshchenov and N. G. Khlebtsov, *ACS Nano*, 2011, **5**, 7077–7089.
4 S.-G. Chen, Y. Yu, X. Zhao, Y. Ma, X.-K. Jiang and Z.-T. Li, *J. Am. Chem. Soc.*, 2011, **133**, 11124–11127.
5 T. Hasobe, H. Imahori, P. V. Kamat, T. K. Ahn, S. K. Kim, D. Kim, A. Fujimoto, T. Hirakawa and S. Fukuzumi, *J. Am. Chem. Soc.*, 2004, **127**, 1216–1228.
6 C. M. Drain, G. Smeureanu, S. Patel, X. Gong, J. Garno and J. Arijeloye, *New J. Chem.*, 2006, **30**, 1834–1843.
7 H.-X. Ji, J.-S. Hu and L.-J. Wan, *Chem. Commun.*, 2008, 2653–2655.
8 K. Ogawa and Y. Kobuke, *BioMed Res. Int.*, 2013, **2013**, 125658–125668.
9 K. M. Kadish, K. M. Smith, R. Guilard and Editors, *The Porphyrin Handbook*, Academic Press, San Diego, CA, 2000, vol. 6, p. 346.
10 H. Imahori, T. Umeyama, K. Kurotobi and Y. Takano, *Chem. Commun.*, 2012, **48**, 4032–4045.
11 C. M. Drain, A. Varotto and I. Radivojevic, *Chem. Rev.*, 2009, **109**, 1630–1658.
12 T. Hasobe, *Phys. Chem. Chem. Phys.*, 2010, **12**, 44–57.

13 T. Hasobe, *J. Phys. Chem. Lett.*, 2013, **4**, 1771–1780.
14 T. Hasobe, H. Sakai, K. Mase, K. Ohkubo and S. Fukuzumi, *J. Phys. Chem. C*, 2013, **117**, 4441–4449.
15 C. C. Rich and J. L. McHale, *Phys. Chem. Chem. Phys.*, 2012, **14**, 2362–2374.
16 P. Guo, P. Chen, W. Ma and M. Liu, *J. Mater. Chem.*, 2012, **22**, 20243–20249.
17 P. Guo, P. Chen and M. Liu, *ACS Appl. Mater. Interfaces*, 2013, **5**, 5336–5345.
18 S. Mandal, S. K. Nayak, S. Mallampalli and A. Patra, *ACS Appl. Mater. Interfaces*, 2014, **6**, 130–136.
19 S. C. Doan, S. Shanmugham, D. E. Aston and J. L. McHale, *J. Am. Chem. Soc.*, 2005, **127**, 5885–5892.
20 J.-J. Wu, N. Li, K.-A. Li and F. Liu, *J. Phys. Chem. B*, 2008, **112**, 8134–8138.
21 L. Zhang, Y. Tian and M. Liu, *Phys. Chem. Chem. Phys.*, 2011, **13**, 17205–17209.
22 M. Ali, V. Kumar, S. N. Baker, G. A. Baker and S. Pandey, *Phys. Chem. Chem. Phys.*, 2010, **12**, 1886–1894.
23 P. Dutta, R. Rai and S. Pandey, *J. Phys. Chem. B*, 2011, **115**, 3578–3587.
24 X. Duan, J. Ma, J. Lian and W. Zheng, *CrystEngComm*, 2014, **16**, 2550–2559.
25 M. Antonietti, D. Kuang, B. Smarsly and Y. Zhou, *Angew. Chem., Int. Ed.*, 2004, **43**, 4988–4992.
26 Y.-J. Zhu, W.-W. Wang, R.-J. Qi and X.-L. Hu, *Angew. Chem., Int. Ed.*, 2004, **43**, 1410–1414.
27 J. Ma, L. Chang, J. Lian, Z. Huang, X. Duan, X. Liu, P. Peng, T. Kim, Z. Liu and W. Zheng, *Chem. Commun.*, 2010, **46**, 5006–5008.
28 J. G. Huddleston, A. E. Visser, W. M. Reichert, H. D. Willauer, G. A. Broker and R. D. Rogers, *Green Chem.*, 2001, **3**, 156–164.
29 S. Kundu, A. Kar and A. Patra, *J. Lumin.*, 2012, **132**, 1400–1406.
30 A. Kar, S. Kundu and A. Patra, *RSC Adv.*, 2012, **2**, 4879–4885.
31 L. A. Estroff and A. D. Hamilton, *Chem. Rev.*, 2004, **104**, 1201–1217.
32 J.-H. Ryu and M. Lee, *J. Am. Chem. Soc.*, 2005, **127**, 14170–14171.
33 M. Ikeda, M. Takeuchi and S. Shinkai, *Chem. Commun.*, 2003, 1354–1355.
34 E. Lee, J.-K. Kim and M. Lee, *Angew. Chem., Int. Ed.*, 2008, **47**, 6375–6378.
35 L. Chen, S. Revel, K. Morris and D. J. Adams, *Chem. Commun.*, 2010, **46**, 4267–4269.
36 M. Kasha, *Radiat. Res.*, 1963, **20**, 55–70.
37 I. Radivojevic, G. Bazzan, B. P. Burton-Pye, K. Ithisuphalap, R. Saleh, M. F. Durstock, L. C. Francesconi and C. M. Drain, *J. Phys. Chem. C*, 2012, **116**, 15867–15877.
38 Z. Zhao, T. Nyokong and M. D. Maree, *Dalton Trans.*, 2005, 3732–3737.
39 S. Tannert, E. A. Ermilov, J. O. Vogel, M. T. M. Choi, D. K. P. Ng and B. Röder, *J. Phys. Chem. B*, 2007, **111**, 8053–8062.
40 E. A. Ermilov, S. Tannert, T. Werncke, M. T. M. Choi, D. K. P. Ng and B. Roeder, *Chem. Phys.*, 2006, **328**, 428–437.
41 A. C. S. Samia, X. Chen and C. Burda, *J. Am. Chem. Soc.*, 2003, **125**, 15736–15737.
42 X. Shen, F. He, J. Wu, G. Q. Xu, S. Q. Yao and Q.-H. Xu, *Langmuir*, 2011, **27**, 1739–1744.
43 S. Bhattacharyya, M. K. Barman, A. Baidya and A. Patra, *J. Phys. Chem. C*, 2014, **118**, 9733–9740.
44 L. M. Rossi, P. R. Silva, L. L. R. Vono, A. U. Fernandes, D. B. Tada and M. S. Baptista, *Langmuir*, 2008, **24**, 12534–12538.
45 C.-Y. Chen, Y. Tian, Y.-J. Cheng, A. C. Young, J.-W. Ka and A. K. Y. Jen, *J. Am. Chem. Soc.*, 2007, **129**, 7220–7221.
46 M. Kuruppuarachchi, H. Savoie, A. Lowry, C. Alonso and R. W. Boyle, *Mol. Pharmaceutics*, 2011, **8**, 920–931.
47 S. Ishihara, J. Labuta, W. Van Rossom, D. Ishikawa, K. Minami, J. P. Hill and K. Ariga, *Phys. Chem. Chem. Phys.*, 2014, **16**, 9713–9746.
48 R. Chitta, A. S. D. Sandanayaka, A. L. Schumacher, L. D'Souza, Y. Araki, O. Ito and F. D'Souza, *J. Phys. Chem. C*, 2007, **111**, 6947–6955.
49 J. W. Walton, A. Bourdolle, S. J. Butler, M. Soulie, M. Delbianco, B. K. McMahon, R. Pal, H. Puschmann, J. M. Zwier, L. Lamarque, O. Maury, C. Andraud and D. Parker, *Chem. Commun.*, 2013, **49**, 1600–1602.
50 D. Brevet, M. Gary-Bobo, L. Raehm, S. Richeter, O. Hocine, K. Amro, B. Loock, P. Couleaud, C. Frochot, A. Morere, P. Maillard, M. Garcia and J.-O. Durand, *Chem. Commun.*, 2009, 1475–1477.
51 R. S. Varma and V. V. Namboodiri, *Chem. Commun.*, 2001, 643–644.
52 E. Dinda, S. Si, A. Kotal and T. K. Mandal, *Chem.–Eur. J.*, 2008, **14**, 5528–5537.
53 X. Gong, T. Milic, C. Xu, J. D. Batteas and C. M. Drain, *J. Am. Chem. Soc.*, 2002, **124**, 14290–14291.
54 D. Tuncel and H. V. Demir, *Nanoscale*, 2010, **2**, 484–494.
55 L. Vurth, C. Hadad, S. Achelle, J. C. Garcia-Martinez, J. Rodriguez-Lopez and O. Stephan, *Colloid Polym. Sci.*, 2012, **290**, 1353–1359.
56 S. Bhattacharyya, T. Sen and A. Patra, *J. Phys. Chem. C*, 2010, **114**, 11787–11795.
57 F. Kong, Y. M. Sun and R. K. Yuan, *Nanotechnology*, 2007, **18**, 265707.
58 S. Mandal, S. Bhattacharyya, V. Borovkov and A. Patra, *J. Phys. Chem. C*, 2011, **115**, 24029–24036.
59 J. R. Lakowicz, *Principles of Fluorescence Spectroscopy*, Kluwer Academic/Plenum Publishers, New York, 3rd edn, 1999, p. 496.
60 S. Mandal, M. Rahaman, S. Sadhu, S. K. Nayak and A. Patra, *J. Phys. Chem. C*, 2013, **117**, 3069–3077.
61 *Porphyrins and Metalloporphyrins*, ed. K. M. Smith, Elsevier, Amsterdam, 1975, p. 910.
62 S. Arnold, W. B. Whitten and A. C. Damask, *Phys. Rev. B: Condens. Matter Mater. Phys.*, 1971, **3**, 3452–3457.
63 M. Kasha, H. R. Rawls and M. A. El-Bayoumi, *Pure Appl. Chem.*, 1965, **11**, 371–392.
64 V. V. Borovkov, J. M. Lintuluoto and Y. Inoue, *J. Am. Chem. Soc.*, 2001, **123**, 2979–2989.

65 O. Ohno, Y. Kaizu and H. Kobayashi, *J. Chem. Phys.*, 1985, **82**, 1779–1787.
66 N. C. Maiti, S. Mazumdar and N. Periasamy, *J. Phys. Chem. B*, 1998, **102**, 1528–1538.
67 S. Verma, A. Ghosh, A. Das and H. N. Ghosh, *J. Phys. Chem. B*, 2010, **114**, 8327–8334.
68 H. Yaku, T. Murashima, D. Miyoshi and N. Sugimoto, *Chem. Commun.*, 2010, **46**, 5740–5742.
69 S. Mandal, S. Bhattacharyya, V. Borovkov and A. Patra, *J. Phys. Chem. C*, 2012, **116**, 11401–11407.
70 P. N. Prasad, *Introduction to biophotonics*, John Wiley & Sons; Inc., Hoboken, NJ, 2003, pp. 203–249.